Conjugated co-polymers of vinylene flanked naphthalene diimide

Zhuping Fei[†], Yang Han[†,‡,*], Jaime Martin[§], Fiona H. Scholes[±], Mohammed Al-Hashimi[‖], Siham Y. AlQaradawi[⊥], Natalie Stingelin[§], Thomas D. Anthopoulos[‡], Martin Heeney[†,*]

[†]Department of Chemistry and Centre for Plastic Electronics, Imperial College London, London SW7 2AZ, UK

[‡]Department of Physics and Centre for Plastic Electronics, Imperial College London, London SW7 2AZ, UK

[§]Department of Materials and Centre for Plastic Electronics, Imperial College London, London SW7 2AZ, UK

[±]CSIRO Manufacturing, Private Bag 10, Clayton South, Victoria 3169, Australia

[⊥]Department of Chemistry & Earth Sciences, Qatar University, P.O. Box 2713 Doha, Qatar

[‖]Department of Chemistry, Texas A&M University at Qatar, P.O. Box 23874, Doha, Qatar

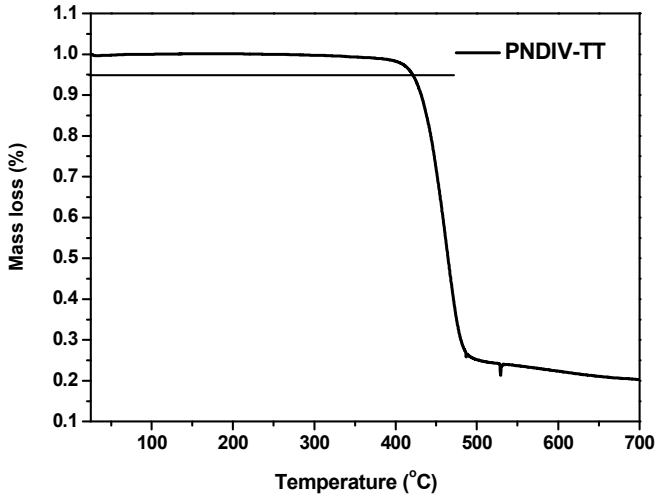

Figure S1. TGA plot of **PNDIV-TT** with a heating rate of 10°C min^{-1} under nitrogen.

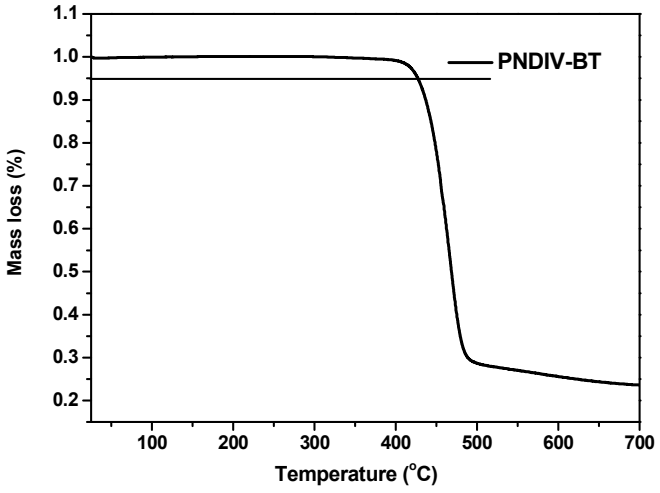

Figure S2. TGA plot of **PNDIV-BT** with a heating rate of 10°C min^{-1} under nitrogen.

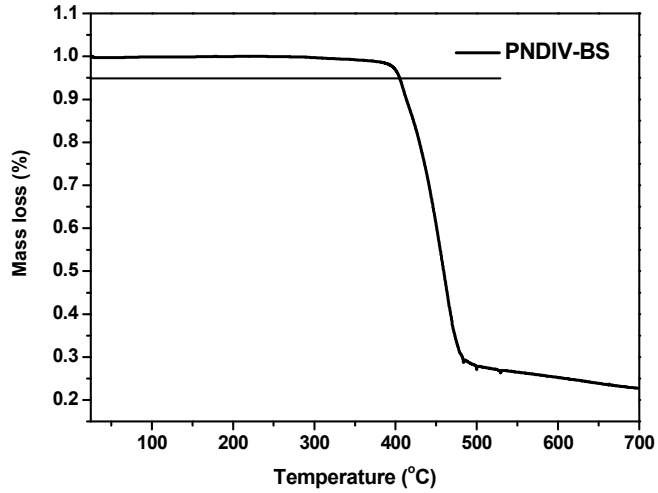

Figure S3. TGA plot of **PNDIV-BS** with a heating rate of 10°C min^{-1} under nitrogen.

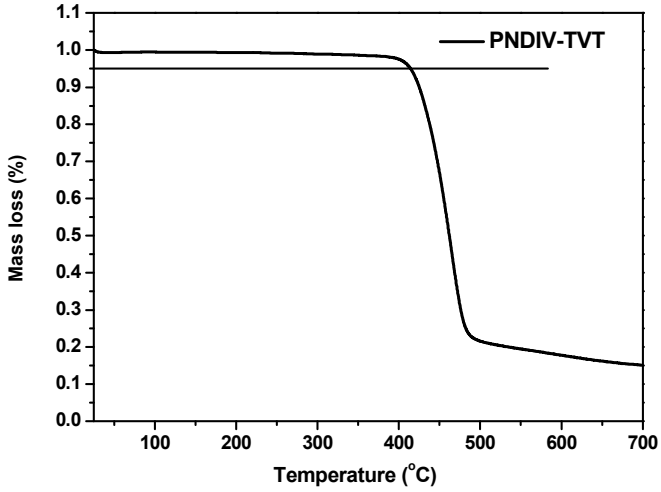

Figure S4. TGA plot of **PNDIV-TVT** with a heating rate of 10°C min^{-1} under nitrogen.

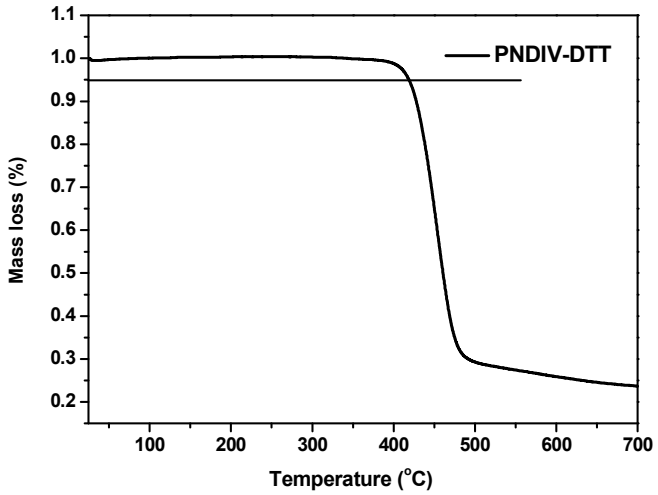

Figure S5. TGA plot of **PNDIV-DTT** with a heating rate of 10°C min^{-1} under nitrogen.

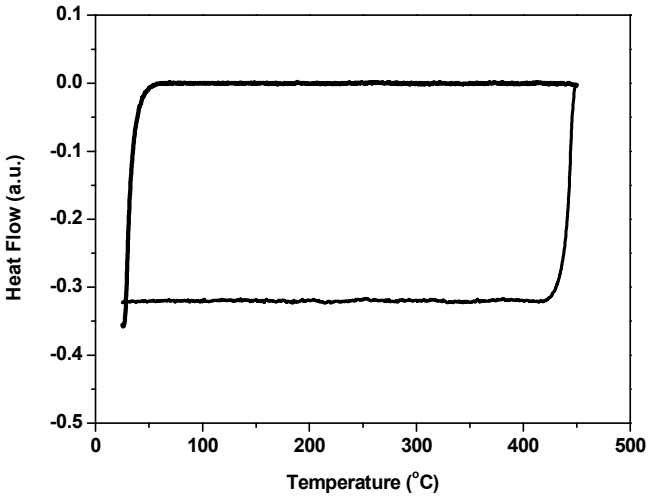

Figure S6. Flash DSC trace of **PNDIV-BT** with a heating and cooling rate of 500 K s^{-1}. (Endo up)

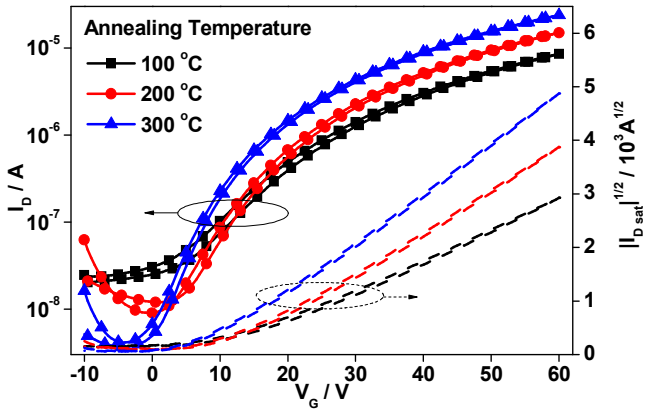

Figure S7. Annealing temperature-dependent transfer characteristics (V_D = 60 V) of **PNDIV-BT** based BG/TC configuration OTFT device with $Ba(OH)_2$ layer between polymer and Au electrode.

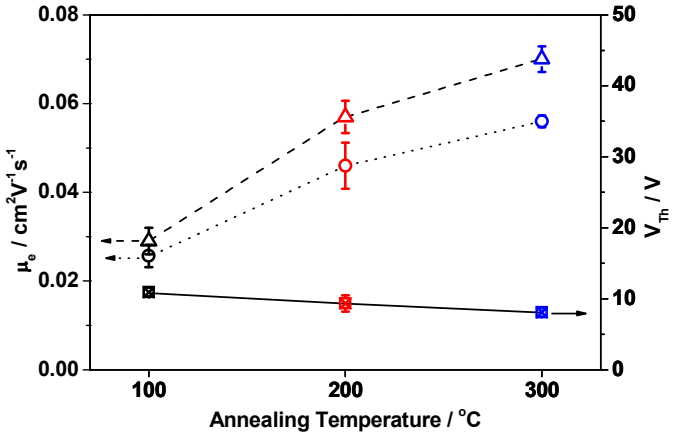

Figure S8. Annealing temperature-dependent device parameters of PNDIV-BT based BG/TC configuration OTFT device with $Ba(OH)_2$ layer between polymer and Au electrode. Saturation mobility at VD = 60 V (triangle); linear mobility at VD = 10 V (circle); and threshold voltage (crossed square).

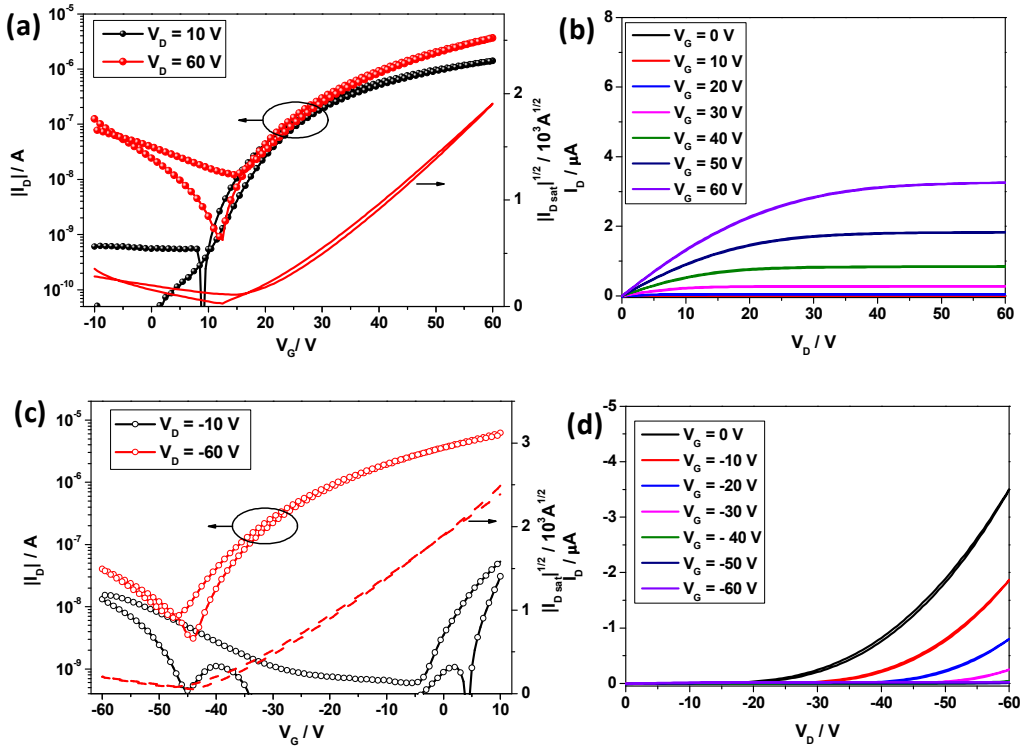

Figure S9. Transfer (a, c) and output (b, d) characteristics of **PNDIV-TT**-based BG/TC configuration OFET device under positive and negative bias. The width and length of the transistor channels are W = 1000 μm and L = 40μm, respectively.

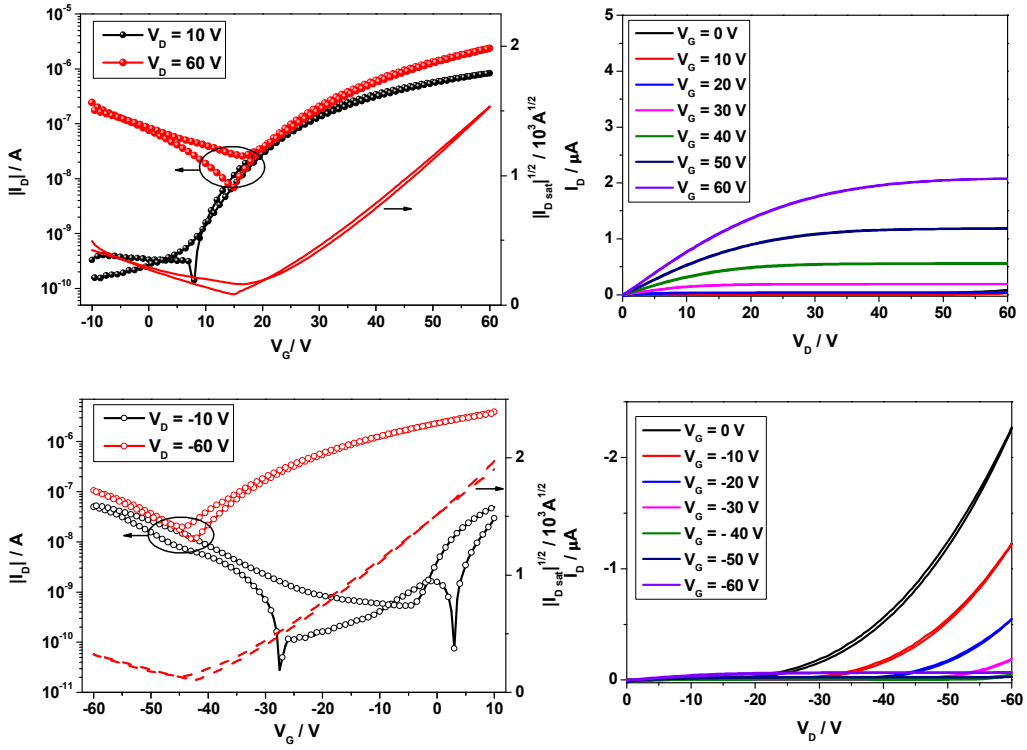

Figure S10. Transfer (a, c) and output (b, d) characteristics of **PNDIV-BS**-based BG/TC configuration OFET device under positive and negative bias. The width and length of the transistor channels are W = 1000 μm and L = 40μm, respectively.

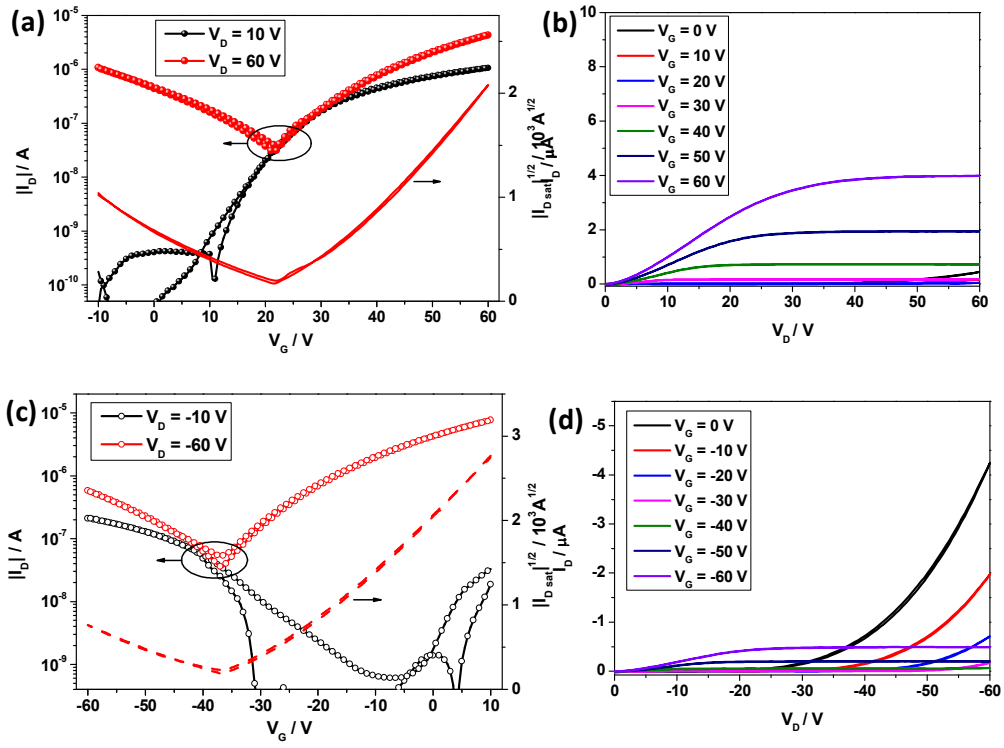

Figure S11. Transfer (a, c) and output (b, d) characteristics of **PNDIV-TVT**-based BG/TC configuration OFET device under positive and negative bias. The width and length of the transistor channels are W = 1000 μm and L = 40μm, respectively.

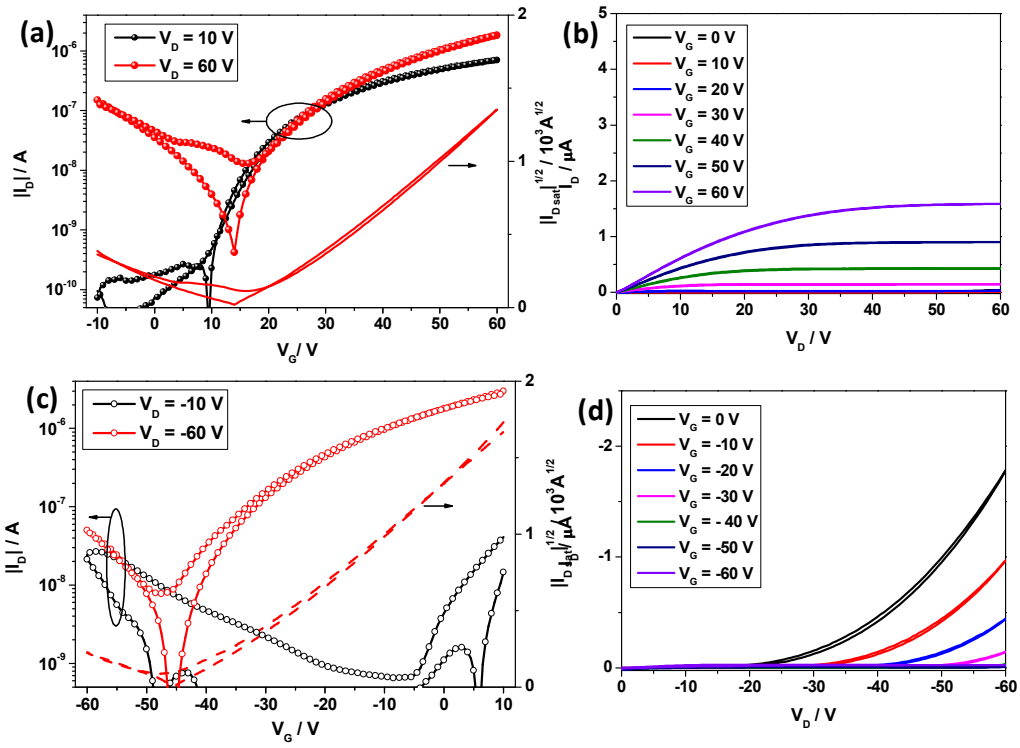

Figure S12. Transfer (a, c) and output (b, d) characteristics of **PNDIV-DTT**-based BG/TC configuration OFET device under positive and negative bias. The width and length of the transistor channels are W = 1000 μm and L = 40μm, respectively.

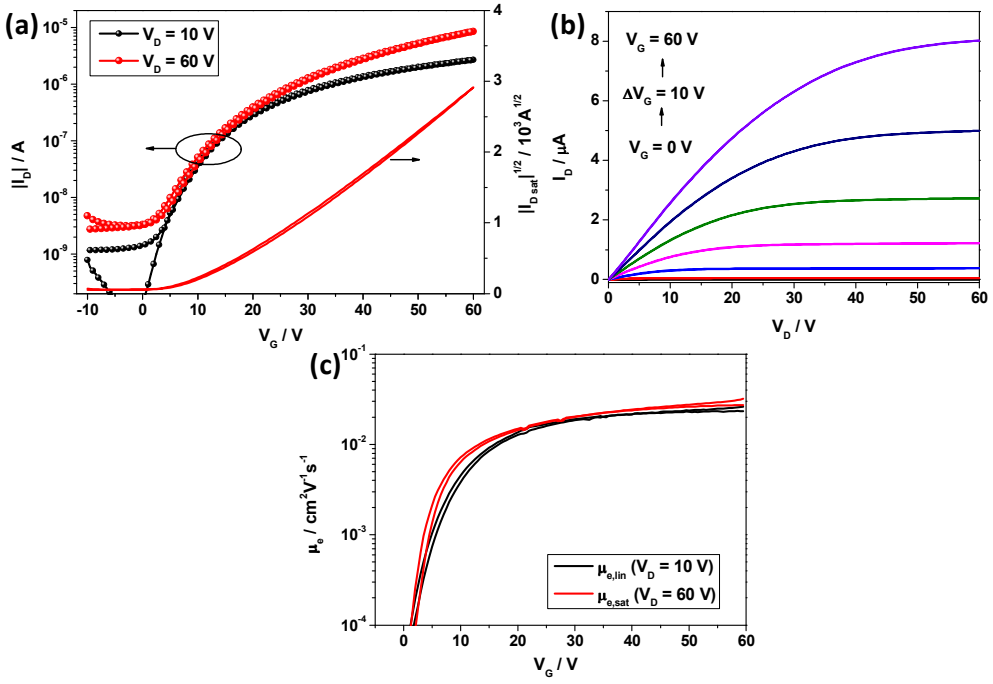

Figure S13. Transfer (a) and output (b) characteristics of **PNDIV-TT**-based BG/TC configuration OFET device with $Ba(OH)_2$ layer between polymer and Au electrode. (c) Mobility calculation based on first derivative of the linear regime transfer curve and first derivative of the square root of the saturation regime transfer curve. The width and length of the transistor channels are W = 1000 μm and L = 40μm, respectively.

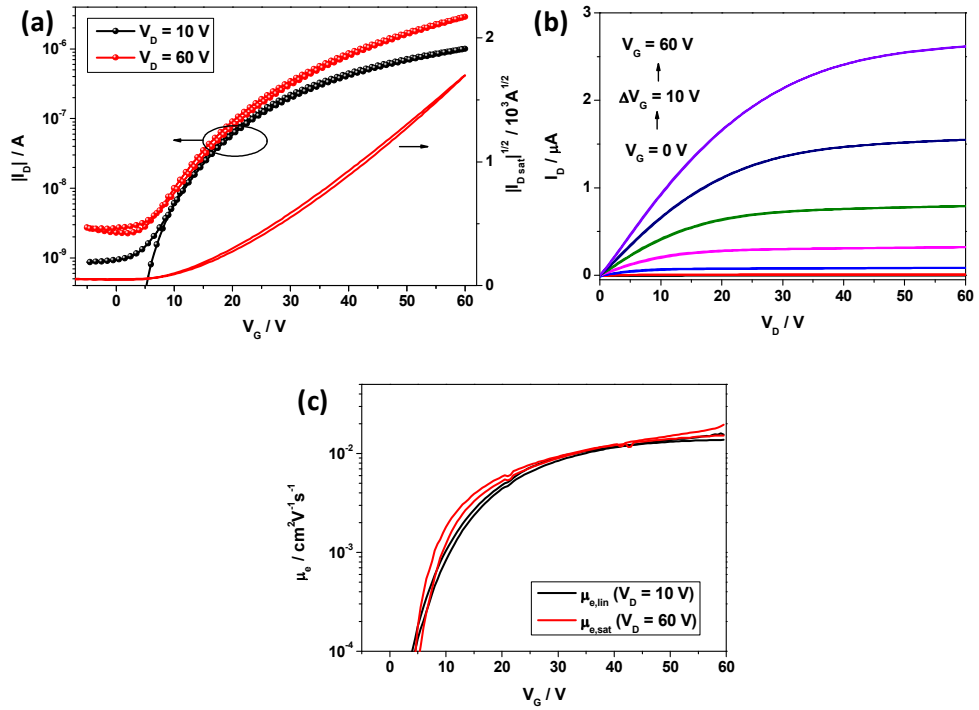

Figure S14. Transfer (a) and output (b) characteristics of **PNDIV-BS**-based BG/TC configuration OFET device with $Ba(OH)_2$ layer between polymer and Au electrode. (c) Mobility calculation based on first derivative of the linear regime transfer curve and first derivative of the square root of the saturation regime transfer curve. The width and length of the transistor channels are $W = 1000$ μm and $L = 40$μm, respectively.

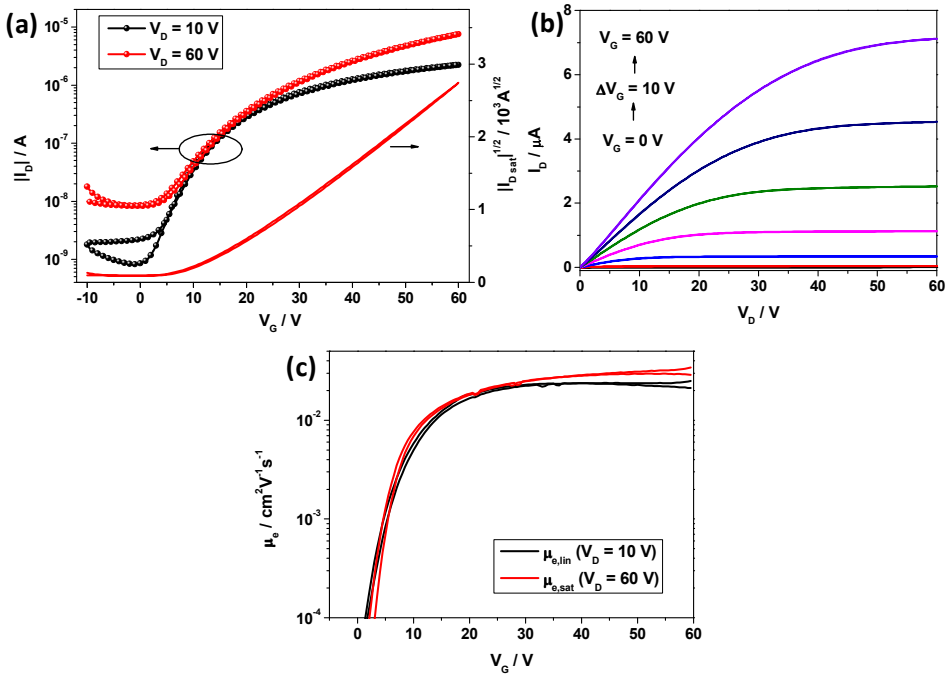

Figure S15. Transfer (a) and output (b) characteristics of **PNDIV-TVT**-based BG/TC configuration OFET device with $Ba(OH)_2$ layer between polymer and Au electrode. (c) Mobility calculation based on first derivative of the linear regime transfer curve and first derivative of the square root of the saturation regime transfer curve. The width and length of the transistor channels are W = 1000 μm and L = 40μm, respectively.

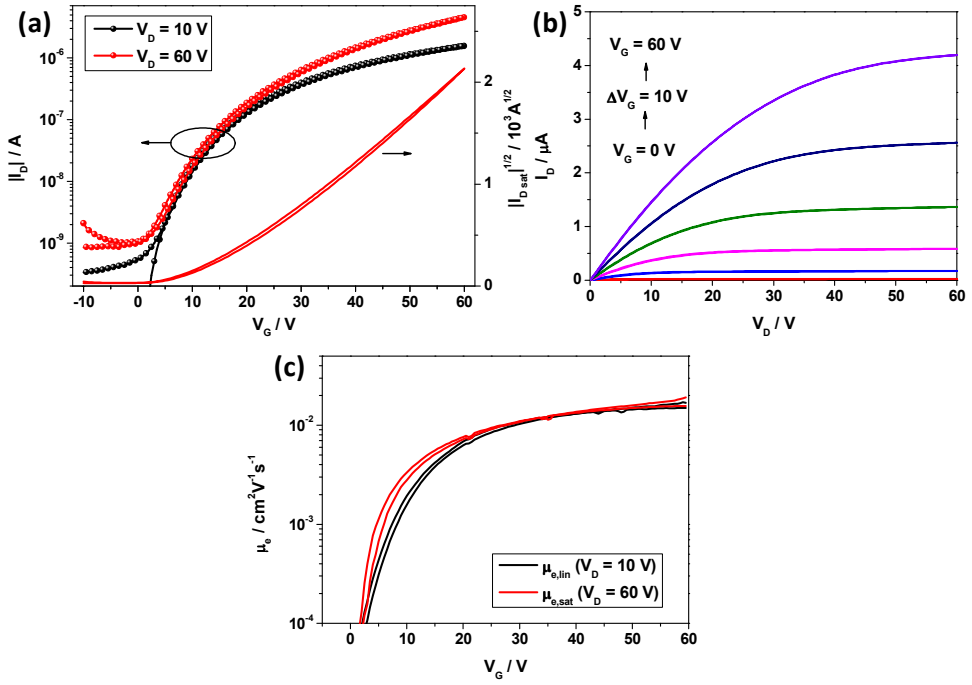

Figure S16. Transfer (a) and output (b) characteristics of **PNDIV-DTT**-based BG/TC configuration OFET device with $Ba(OH)_2$ layer between polymer and Au electrode. (c) Mobility calculation based on first derivative of the linear regime transfer curve and first derivative of the square root of the saturation regime transfer curve. The width and length of the transistor channels are W = 1000 μm and L = 40μm, respectively.

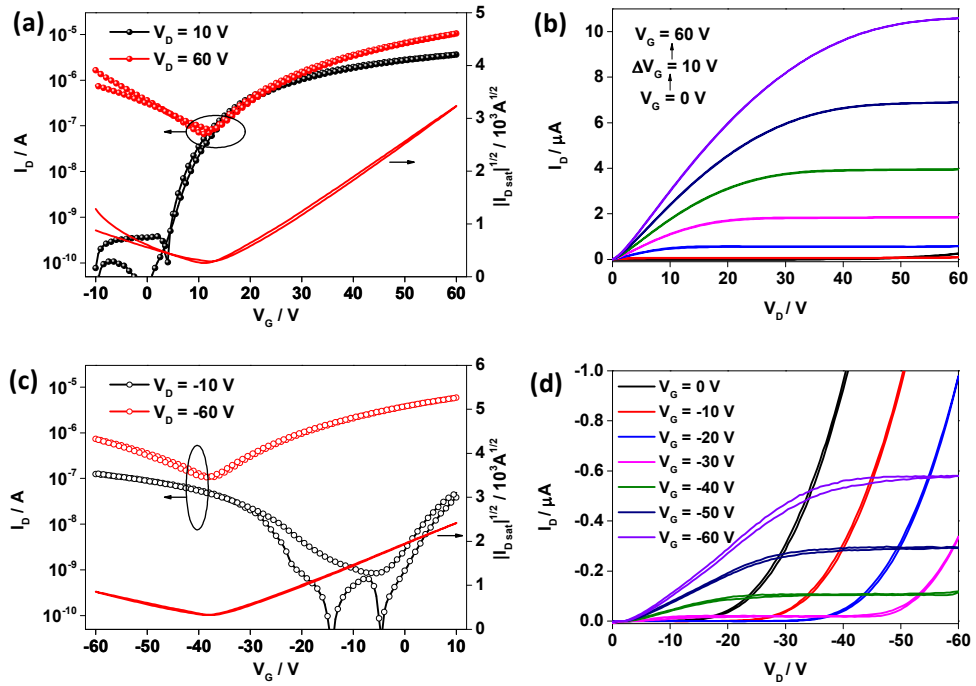

Figure S17. Transfer (a, c) and output (b, d) characteristics of PNDIV-BT-based BG/TC configuration OTFT device under positive and negative bias. The polymer film was annealed at 300 °C then treated with drop cast methanol instead of methanolic $Ba(OH)_2$.

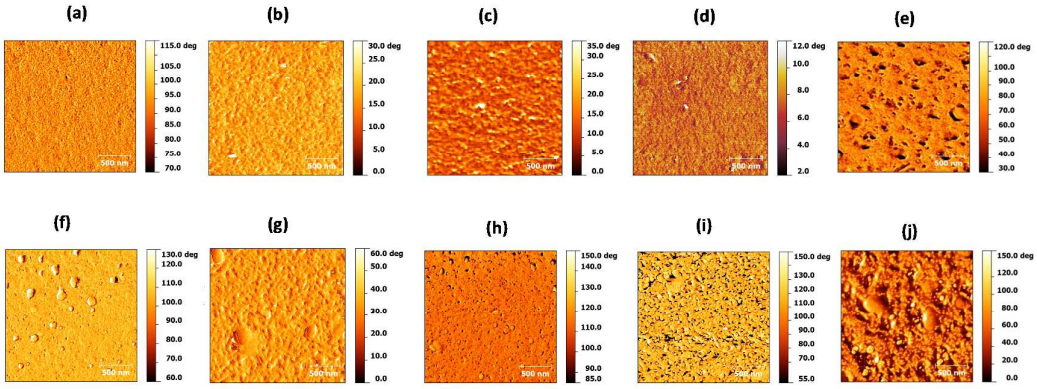

Figure S18. Phase images of **PNDIV-TT**, **PNDIV-BT**, **PNDIV-BS**, **PNDIV-TVT** and **PNDIV-DTT** in bottom-gate top-contact configuration without $Ba(OH)_2$ layer (a-e), and with $Ba(OH)_2$ layer (f-j) between polymer and Au electrode.

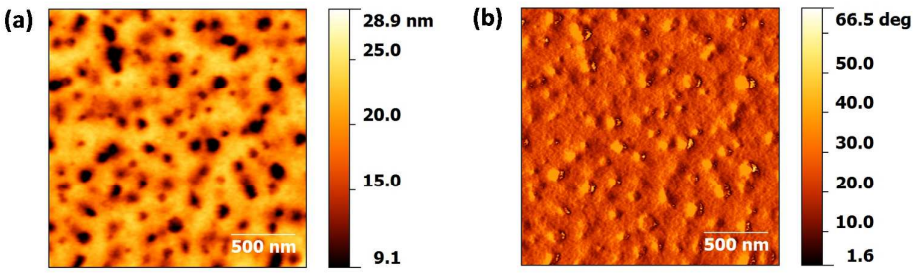

Figure S19. AFM topography (a) and phase (b) images of **PNDIV-DTT** film annealed at 100 °C for 1-2 min. Pin holes were already developed at this relatively low annealing temperature.

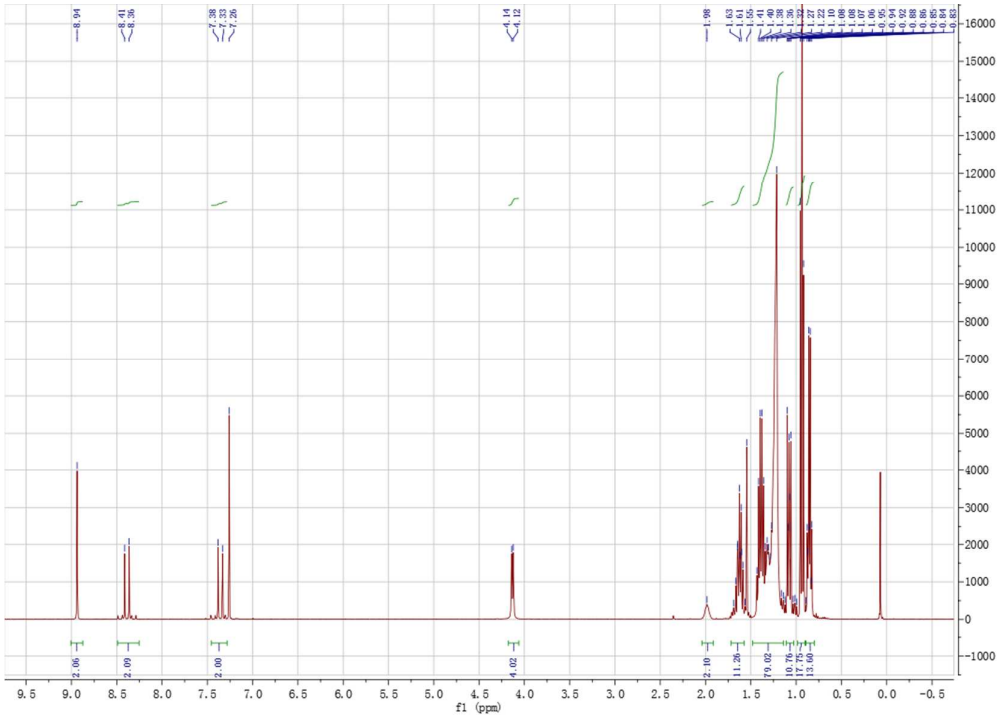

Figure S20. The ^{1}H NMR spectrum of monomer **2** in CDCl3 at RT.

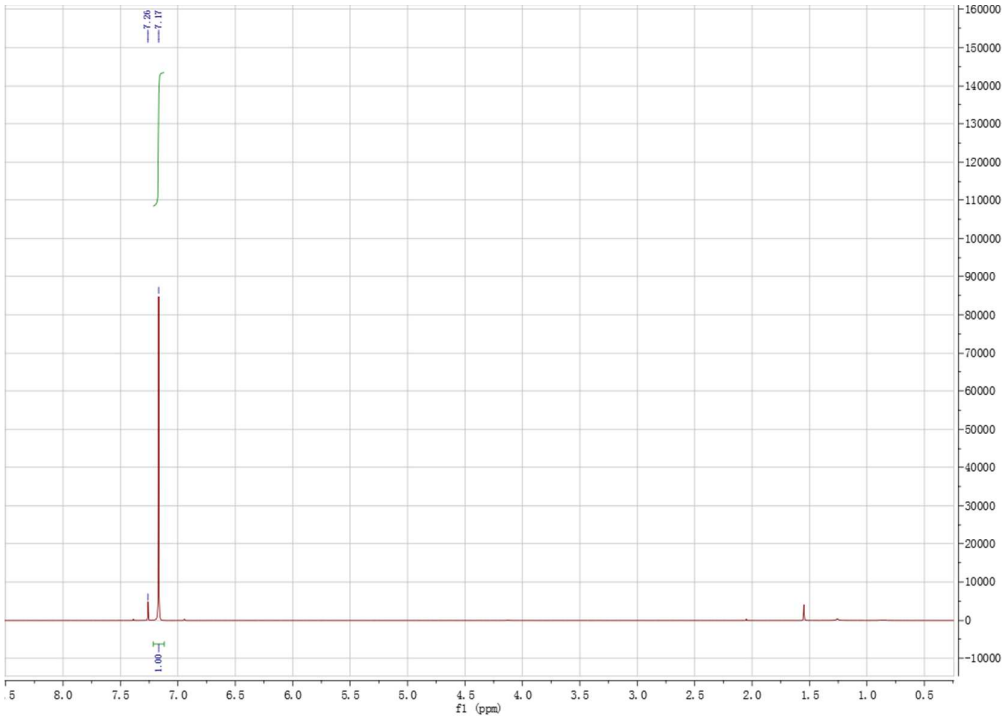

Figure S21. The ^{1}H NMR spectrum of 2,5-dibromothieno[3,2-b]thiophene in CDCl3 at RT.

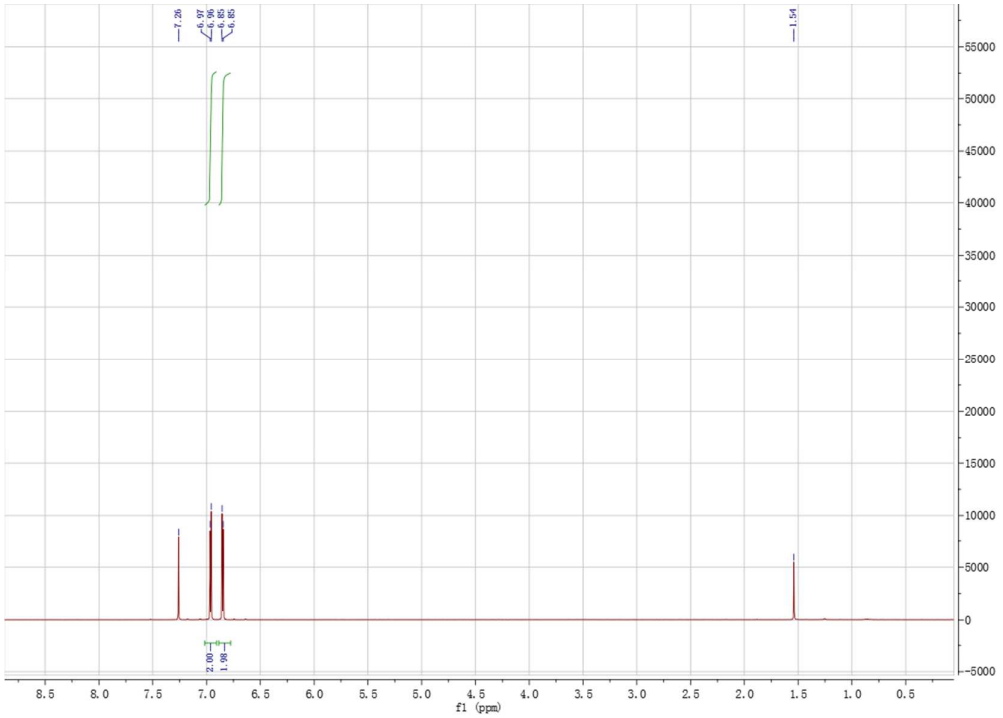

Figure S22. The ^{1}H NMR spectrum of 5,5'-dibromo-2,2'-bithiophene in CDCl3 at RT.

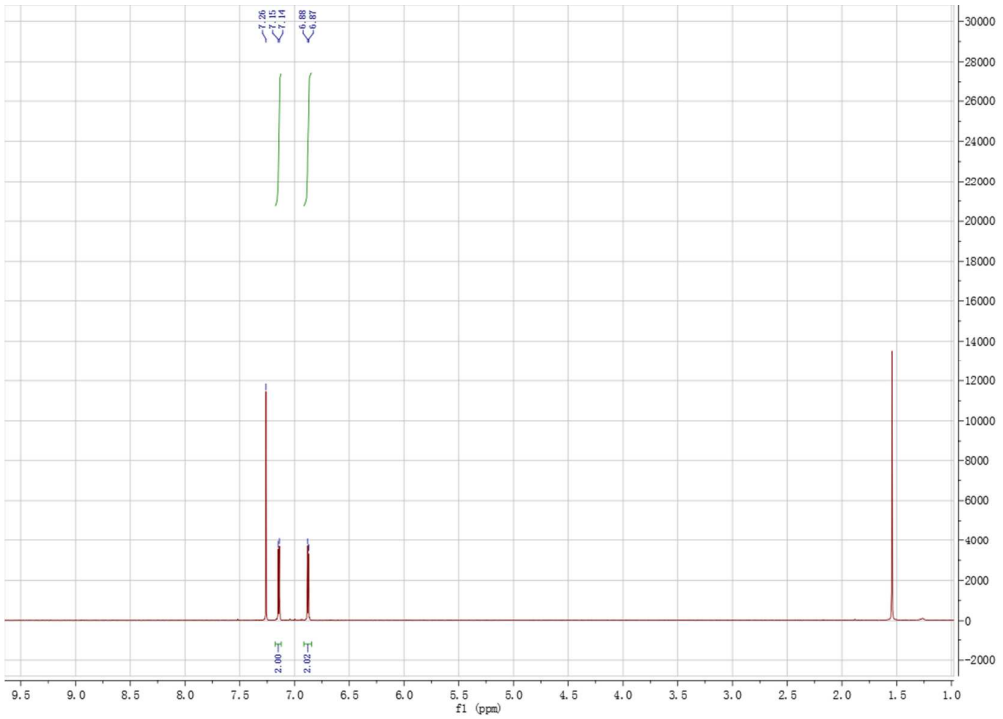

Figure S23. The ^{1}H NMR spectrum of 5,5'-dibromo-2,2'-biselenophene in CDCl3 at RT.

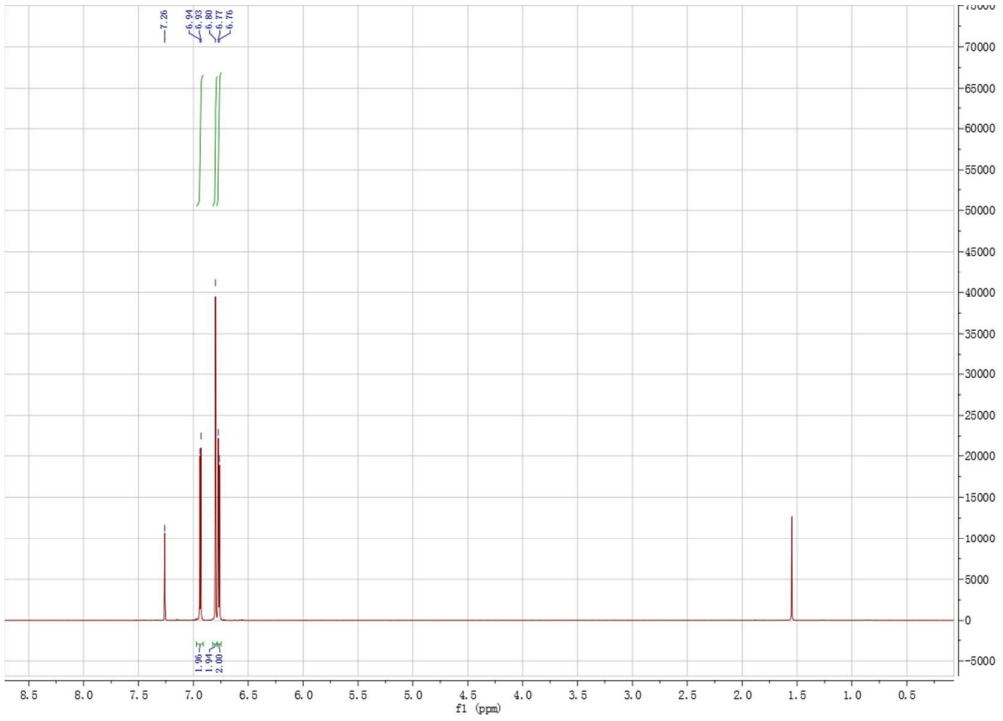

Figure S24. The ^{1}H NMR spectrum of (E)-1,2-bis(5-bromothiophen-2-yl)ethane in CDCl3 at RT.

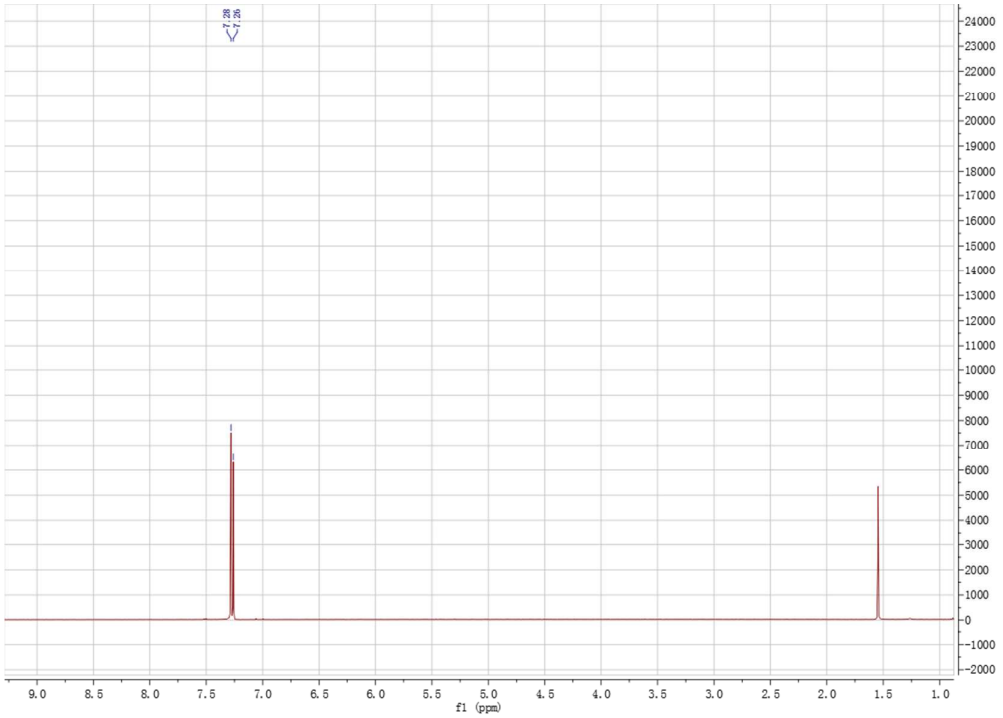

Figure S25. The ^{1}H NMR spectrum of 2,6-dibromodithieno[3,2-b:2',3'-d]thiophene in CDCl3 at RT.

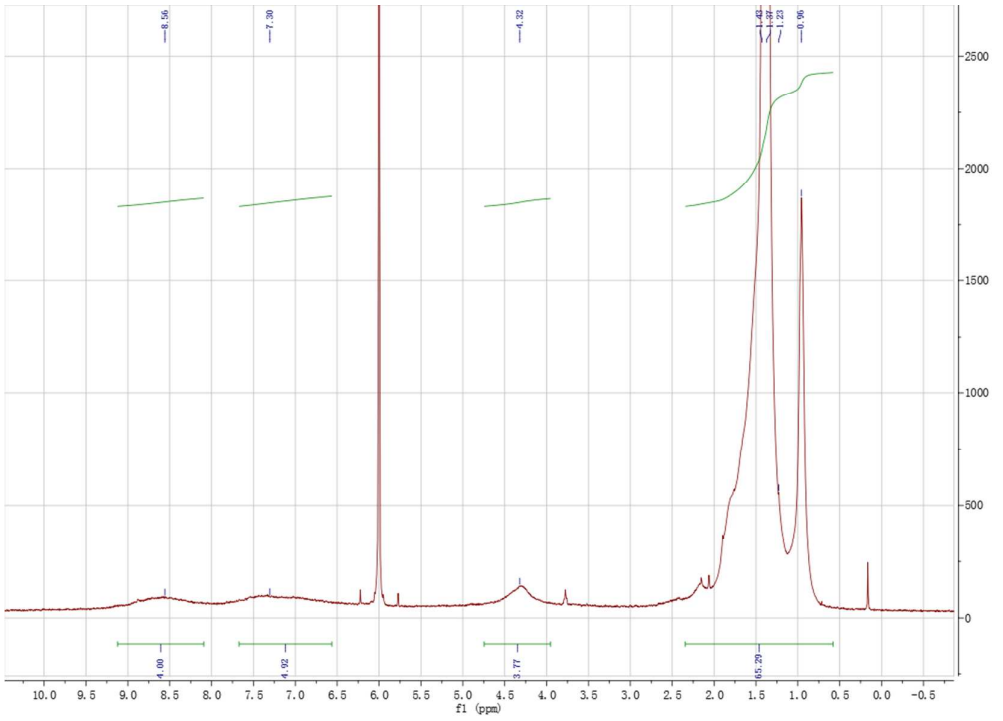

Figure S26. The ^{1}H NMR spectrum of **PNDIV-TT** in *d*-1,1,2,2-tetrachloroethane at 130 °C.

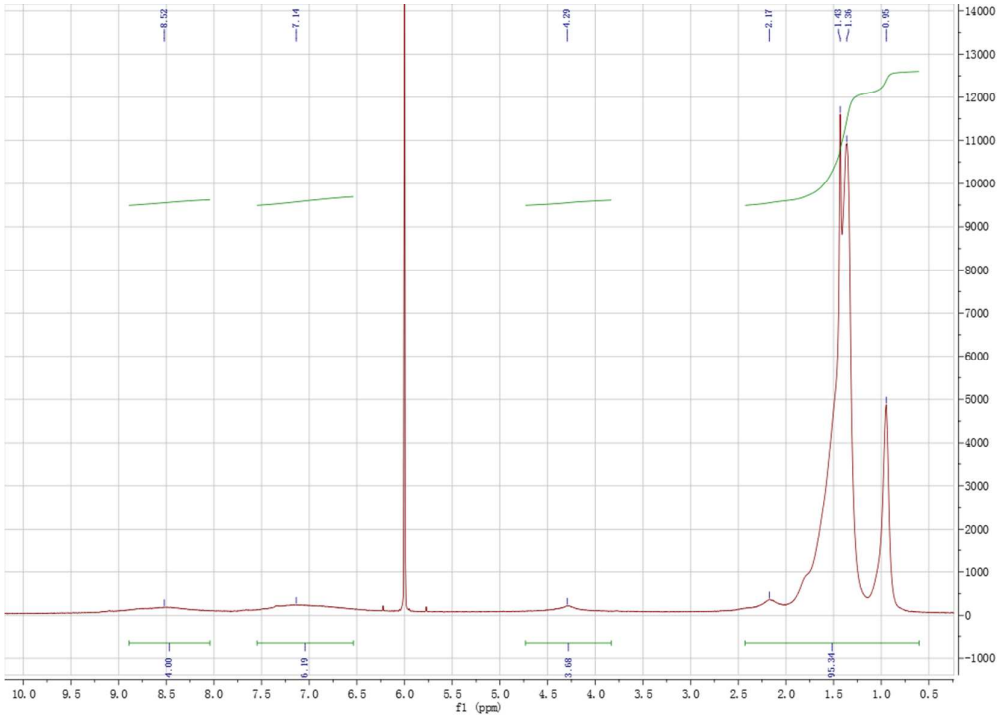

Figure S27. The ^{1}H NMR spectrum of **PNDIV-BT** in *d*-1,1,2,2-tetrachloroethane at 130 °C.

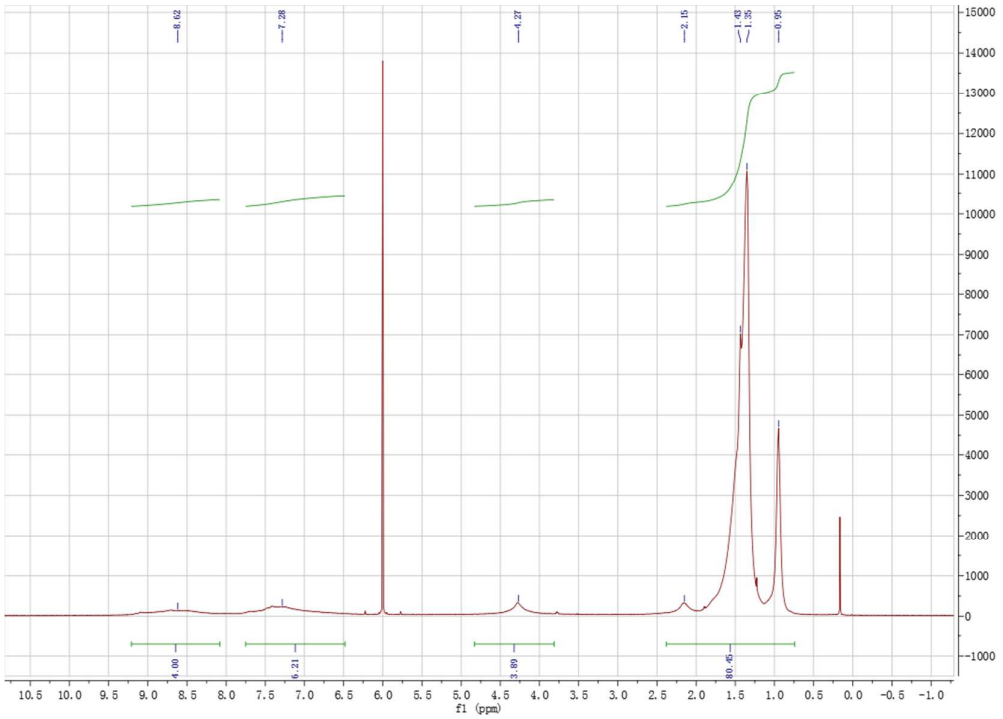

Figure S28. The ^{1}H NMR spectrum of **PNDIV-BS** in *d*-1,1,2,2-tetrachloroethane at 130 °C.

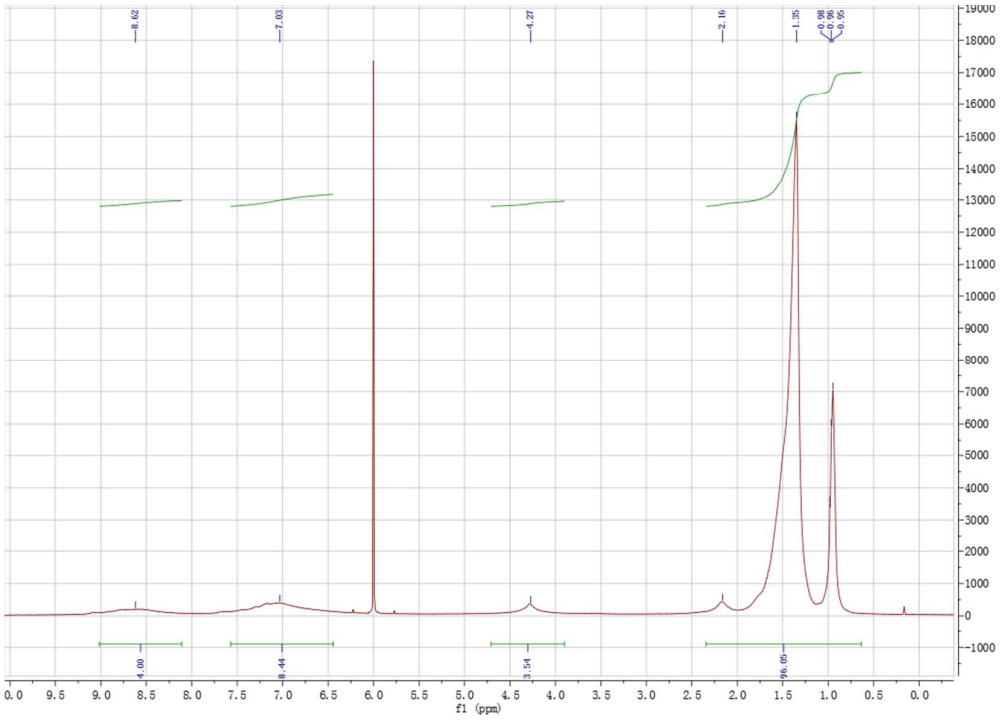

Figure S29. The ^{1}H NMR spectrum of **PNDIV-TVT** in *d*-1,1,2,2-tetrachloroethane at 130 °C.

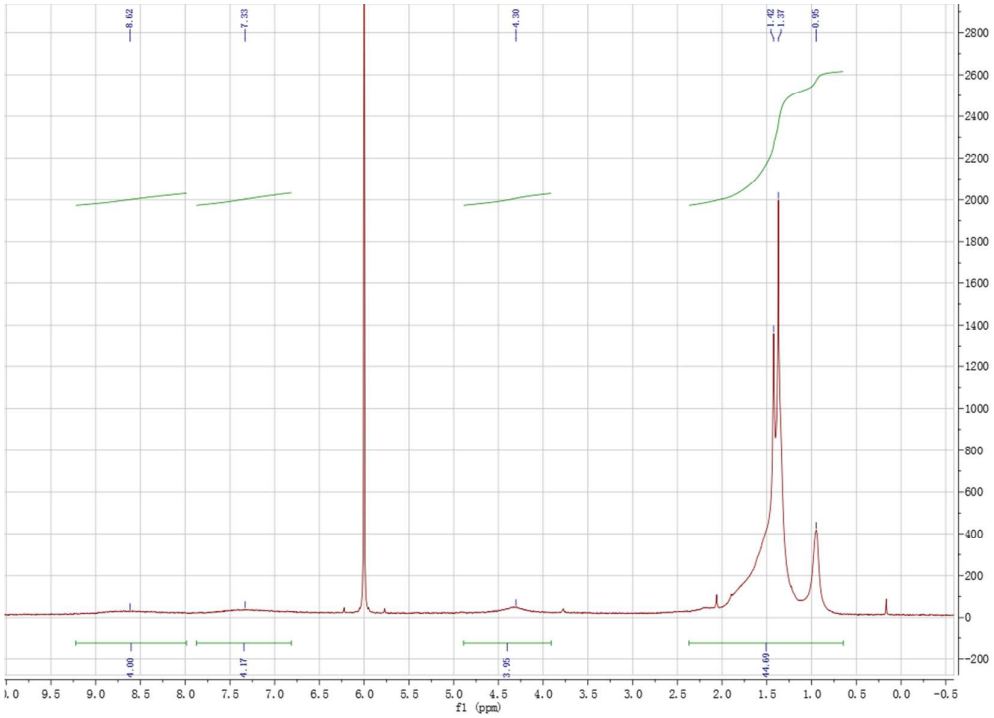

Figure S30. The ^{1}H NMR spectrum of **PNDIV-DTT** in *d*-1,1,2,2-tetrachloroethane at 130 °C.